



# On-Surface Synthesis of a Dicationic Diazahexabenzocoronene Derivative on the Au(111) Surface

Kalyan Biswas, José I. Urgel,\* Kun Xu, Ji Ma, Ana Sánchez-Grande, Pingo Mutombo, Aurelio Gallardo, Koen Lauwaet, Benjamin Mallada, Bruno de la Torre, Adam Matěj, José M. Gallego, Rodolfo Miranda, Pavel Jelínek,\* Xinliang Feng,\* and David Ćija\*

**Abstract:** The atomically precise control over the size, shape and structure of nanographenes (NGs) or the introduction of heteroatom dopants into their  $sp^2$ -carbon lattice confer them valuable electronic, optical and magnetic properties. Herein, we report on the design and synthesis of a hexabenzocoronene derivative embedded with graphitic nitrogen in its honeycomb lattice, achieved via on-surface assisted cyclodehydrogenation on the Au(111) surface. Combined scanning tunnelling microscopy/spectroscopy and non-contact atomic force microscopy investigations unveil the chemical and electronic structures of the obtained dicationic NG. Kelvin probe force microscopy measurements reveal a considerable variation of the local contact potential difference toward lower values with respect to the gold surface, indicative of its positive net charge. Altogether, we introduce the concept of cationic nitrogen doping of NGs on surfaces, opening new avenues for the design of novel carbon nanostructures.

## Introduction

After the revolutionary discovery by Geim and Novoselov in 2004,<sup>[1]</sup> graphene has attracted an enormous interest in science and technology communities, being exhaustively investigated due to its exceptional electronic, mechanical and optical properties.<sup>[2–6]</sup> Despite its potential toward applications, significant drawbacks such as zero band gap, susceptibility to oxidative environments or tendency to

aggregation between graphene layers, among others, have constrained seriously its practical applications. In particular, the high probability of structural defects in the  $sp^2$ -carbon lattice modifies its properties, which may affect the envisioned applications.

In this context, the design and synthesis of atomically precise graphene nanostructures, that is, nanographenes (NGs) that can be bottom-up synthesized through methods available in contemporary synthetic organic chemistry, have recently gained increasing attention.<sup>[7,8]</sup> For instance, NGs may serve as models for investigating the physicochemical properties of graphene and, along with the development of miniaturized and scaled up devices, they have emerged as excellent material candidates toward the engineering of graphene-based devices with great potential in nanoelectronics, optoelectronics and spintronics.<sup>[9,10]</sup> In the last decades, organic chemists have been able to synthesize a wide variety of NGs with different sizes, symmetries and edge structures, taking advance of high-yielding and extensible synthetic methods frequently based on the intramolecular oxidative cyclodehydrogenation reaction of oligophenylene precursors.<sup>[7,11]</sup> However, the decreasing solubility as the size of the NG augments is repeatedly a problem that hampers their synthesis in solution, purification and characterization. In view of these limitations, the synthesis of well-defined NGs has recently been expanded to single-crystal metal surfaces under ultra-high vacuum (UHV) conditions. Herein, the

[\*] K. Biswas, Dr. J. I. Urgel, Dr. A. Sánchez-Grande, Dr. K. Lauwaet, Prof. R. Miranda, Prof. D. Ćija  
IMDEA Nanoscience  
C/ Faraday 9, Campus de Cantoblanco, 28049 Madrid (Spain)  
E-mail: jose-ignacio.urgel@imdea.org  
david.ecija@imdea.org  
Dr. K. Xu, Dr. J. Ma, Prof. X. Feng  
Center for Advancing Electronics and Faculty of Chemistry and Food Chemistry, Technical University of Dresden  
01062 Dresden (Germany)  
E-mail: xinliang.feng@tu-dresden.de  
Dr. P. Mutombo, A. Gallardo, B. Mallada, Dr. B. de la Torre, A. Matěj, Prof. P. Jelínek  
Institute of Physics of the Czech Academy of Science  
CZ-16253 Praha (Czech Republic)  
E-mail: jelinekp@fzu.cz  
A. Gallardo  
Department of Condensed Matter Physics, Faculty of Mathematics and Physics, Charles University  
CZ-180 00 Praha (Czech Republic)

B. Mallada, Dr. B. de la Torre, A. Matěj, Prof. P. Jelínek  
Regional Centre of Advanced Technologies and Materials, Palacký University Olomouc  
CZ-771 46 Olomouc (Czech Republic)  
Dr. J. M. Gallego  
Instituto de Ciencia de Materiales de Madrid, CSIC  
Cantoblanco, 28049 Madrid (Spain)  
Prof. R. Miranda  
Departamento de Física de la Materia Condensada, Universidad Autónoma de Madrid  
28049 Madrid (Spain)

Supporting information and the ORCID identification number(s) for the author(s) of this article can be found under:  
https://doi.org/10.1002/anie.202111863.

© 2021 The Authors. Angewandte Chemie International Edition published by Wiley-VCH GmbH. This is an open access article under the terms of the Creative Commons Attribution Non-Commercial NoDerivs License, which permits use and distribution in any medium, provided the original work is properly cited, the use is non-commercial and no modifications or adaptations are made.

development of atomic-resolution scanning tunnelling microscopy (STM) and atomic force microscopy (AFM) with subnanometer resolution<sup>[12,13]</sup> has initiated a new avenue for the synthesis and characterization of NGs that are insoluble and/or unstable in solution.<sup>[14]</sup>

Over the last years, several NGs have been achieved through surface-catalyzed oxidative cyclodehydrogenation of the molecular precursors.<sup>[20–33]</sup> Only recently, the graphene-based chemical toolbox has been extended to the on-surface synthesis of heteroatom-doped NGs. Controlled substitutional doping is an efficient approach to tune the electronic, magnetic and physicochemical properties of graphene-based materials. In particular, nitrogen doping (see Figure 1 for nitrogen-doped NGs (*I–V*) synthesized on surfaces)<sup>[15–19]</sup> offers an accessible doping process and an efficient modulation of the structure and properties of carbon-based nanostructures, while preserving its high electrical conductivity and potential in optical, electronic and catalytic applica-

tions,<sup>[34–37]</sup> taking simultaneously advance from the modified electrical properties and surface reactivity of N-doped sites. Among the different types of nitrogen dopants, the introduction of graphitic nitrogen in the hexagonal lattice of a NG, where N atoms substitute quaternary C atoms, may lead to a cationic charge state, which confers them interesting catalytic activity.<sup>[38–40]</sup> However, a detailed insight into this kind of N-doped NGs synthesized on surfaces is still lacking.

In this article, we report the on-surface synthesis of a novel dicationic diazahexabenzocoronene derivative on a coinage-metal surface under UHV conditions (Scheme 1). To this end, we synthesized 1,1'-(1,4-phenylene)bis(2,4,6-triphenylpyridin-1-ium) ditetrafluoroborate, named precursor **1**, which can be sublimed and transformed to the targeted diazahexabenzocoronene derivative **2** by thermal activation on the gold surface. The chemical structure of **2** was clearly unveiled via STM, scanning tunnelling spectroscopy (STS), non-contact atomic force microscopy (nc-AFM) and local contact potential difference (LCPD) measured by Kelvin probe force microscopy (KPFM), complemented with density functional theory (DFT) calculations and nc-AFM simulations. Notably, our molecular-level insights provide evidence on the positively charged state of **2** on the Au(111) surface, while exhibiting a marked aromatic character. Our results demonstrate the formation of stable cationic heteroatom-doped NGs on surfaces, paving the way for the design and synthesis of carbon nanostructures with cationic nitrogen dopants.

## Results and Discussion

Precursor **1** was synthesized in solution from 2,4,6-triphenylium tetrafluoroborate and *p*-phenylenediamine via Katritzky reaction (see supporting information for synthetic and characterization details). Sublimation of **1** under UHV conditions onto an Au(111) surface held at room temperature and subsequent annealing to 300 °C induces the cyclodehydrogenation reaction of the molecular precursors (see Figure S1 for mass spectrometry analysis and temperature programmed desorption experiments, which gives information about the detection of species related to BF<sub>4</sub><sup>−</sup> after

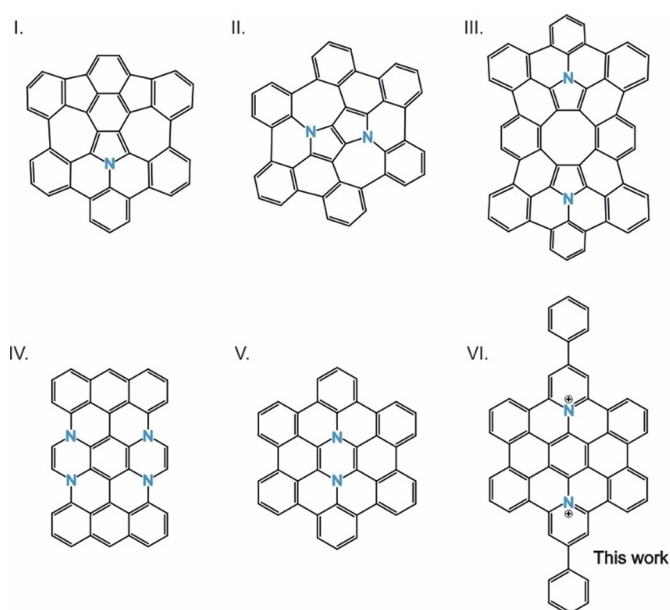
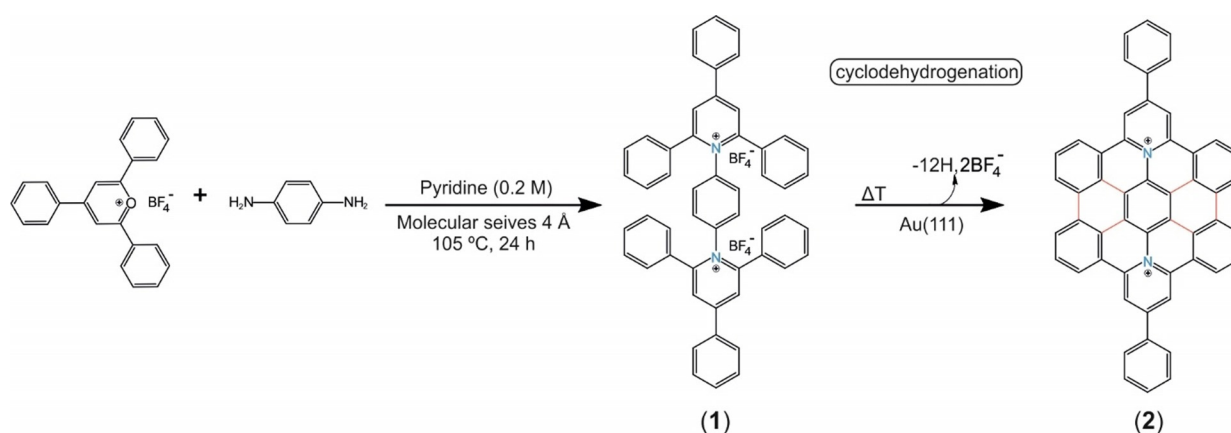


**Figure 1.** Representative synthesis of graphitic nitrogen-doped nanographenes on surfaces (I–VI).<sup>[15–19]</sup>



**Scheme 1.** Solution and on-surface synthesis of the dicationic diphenyl-diazahexabenzocoronene nanographene.

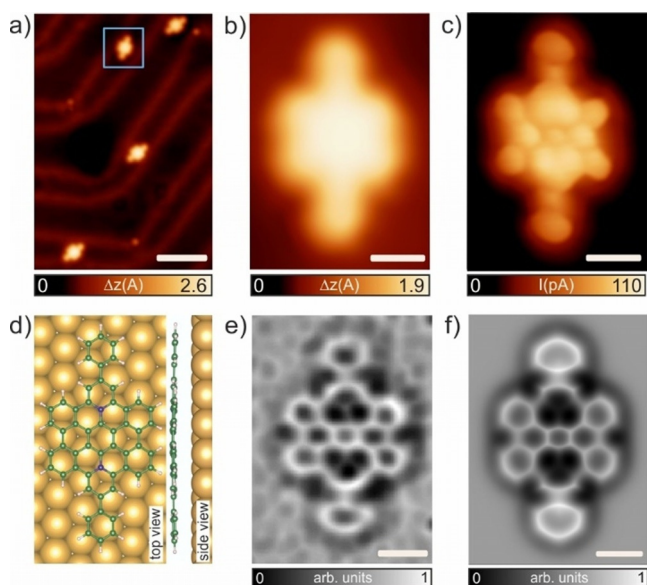


**Figure 2.** On-surface synthesis of diphenyl-diazahexabenzocoronene (**2**) on Au (111). a) Overview STM topographic image after annealing the substrate at 300 °C.  $V_b = 200$  mV,  $I_t = 120$  pA. Scale bar: 5 nm. b) High-resolution constant-current STM image of one of the individual species **2** shown in (a) acquired with a CO-functionalized tip.  $V_b = 10$  mV,  $I_t = 40$  pA. Scale bar: 0.5 nm. c) Constant-height UHR-STM image, acquired with a CO-functionalized tip, revealing the formation of hexagons via cyclodehydrogenation of the molecular precursor **1**.  $V_b = 5$  mV,  $I_t = 30$  pA. Scale bar: 0.5 nm. d) DFT equilibrium geometry of the molecule highlighted in panel (c). Top (left) and side (right) views of the DFT equilibrium geometry of **2** on Au (111). e) Constant-height frequency-shift nc-AFM images of (c) acquired with a CO-functionalized tip. Herein, C–C bonds are undoubtedly identified, while N–C bonds appear at a more negative frequency shift. Z offset = 175 pm above the STM set point: 5 mV, 30 pA. Scale bar: 0.5 nm. f) Calculated frequency shift nc-AFM images of **2** shown in (d). Scale bar: 0.5 nm.

sublimation of **1**). Figure 2a displays a representative large-scale STM image acquired at 4.3 K which shows the presence of individual species on the Au(111) surface. Figure 2b,c show a constant-current STM image and its corresponding constant-height ultrahigh-resolution STM (UHR-STM) image of one of such species, acquired using a carbon monoxide (CO) functionalized tip, which allow us to discern its appearance as planarized nanostructures, confirming the successful intramolecular cyclodehydrogenation of **1** and yielding the synthesis of diphenyl-diazahexabenzocoronene NG (**2**). This is in agreement with the DFT-optimized structure of **2** on Au(111), which reveals a planar adsorption geometry with an adsorption height of 3.2 Å with respect to the underlying surface (Figure 2d). Furthermore, in order to confirm the chemical structure of **2**, we performed nc-AFM measurements. Figure 2e depicts the resulting constant-height frequency-shift image where the carbon-carbon (C–C) bonds are clearly distinguished, while the nitrogen-carbon (N–C) bonds embedded in the NG appear at a darker contrast, that is, more negative frequency shift. Such difference in contrast is attributed to the onset of the short-range repulsive interactions with the CO-tip which occurs first for C atoms and then for N atoms, due to the difference in the van der Waals radius

between C and N, in good correspondence to previously reported works.<sup>[41]</sup> In addition, the simulated nc-AFM image depicted in Figure 2f yields excellent agreement with the experimental image.

Notably, experimental scanning probe measurements combined with theoretical calculations reveal the electronic structure and charged state of **2** on Au(111). First, we have performed STS measurements on **2** in order to explore its electronic structure. Figure 3a shows differential conductance  $dI/dV$  spectra, revealing resonance peaks in the unoccupied density of states at +0.60 V and +1.25 V. These peaks are assigned to the negative ion resonances (NIRs) that derive from the lowest and second lowest unoccupied molecular orbitals (LUMO and LUMO + 1) of **2**, respectively. Constant-current maps of the  $dI/dV$  signal of **2** on Au(111) acquired with a CO-functionalized tip at the energy positions of NIR (LUMO) and NIR + 1 (LUMO + 1) are shown in Figure 3b (left). Next, we have performed calculations of the  $dI/dV$  maps of the dicationic and neutral states of **2** in the gas phase (see Figures 3b and S1). Remarkably, calculated  $dI/dV$  maps of frontier LUMO<sup>(2+)</sup> and LUMO + 1<sup>(2+)</sup> orbitals of the gas phase dication (**2**+) species (Figure 3b, right) match very well with the experimental  $dI/dV$  maps, whereas calculated  $dI/dV$  maps for the neutral species do not (see Figure S2 for the comparison between experimental and calculated  $dI/dV$  maps considering **2** in the neutral state). We consider this as a first evidence on the cationic charge state of **2** on the Au(111) surface. Here, it is worth to mention that a similar protocol has recently been employed to assess the dicationic character of porphyrin-capped graphene nanoribbon segments on Au(111).<sup>[42]</sup>

Our claims about the dicationic charge state of **2** on Au(111) are further supported by a detailed analysis of the DFT calculations. We have studied what charge state a neutral form of **2** would like to keep when deposited on the metallic surface. It is an indirect, but conclusive, way to assess if the dicationic charge state of **2** is stable on the metallic support. First, the frontier HOMO<sup>(n)</sup> orbital of the neutral molecule **2** in the gas phase is located −3.4 eV below the vacuum level. This means it would be positioned ≈0.8 eV above the Fermi level of the Au(111) surface (work function of Au(111) ≈4.5 eV), which points towards a strong tendency of a neutral species to transfer charge to Au(111). Second, DFT calculations of the neutral species **2** on Au(111) surface show significant charge transfer from the molecule to the surface. Namely, the spatial distribution of the charge loss from **2** matches with the spatial distribution of the HOMO<sup>(n)</sup> of the neutral or equivalently the LUMO<sup>(2+)</sup> of the dicationic species (see Figure S3). Figure 3c depicts the comparison between the projected density of states (PDOS) of the free standing neutral species **2** and the PDOS of **2** on the Au(111) surface (top and bottom panel, respectively), which also provides evidence of a substantial charge transfer from the neutral molecule to the metal surface. Herein, the Fermi level crossing of the HOMO<sup>(n)</sup> orbital, being located relatively far away from the Fermi level, strongly supports the presence of the dicationic (**2**+) molecule on the Au(111) surface. Note that though we were able to visualize the negative ion resonances, the detection of any positive ion resonance (PIR)



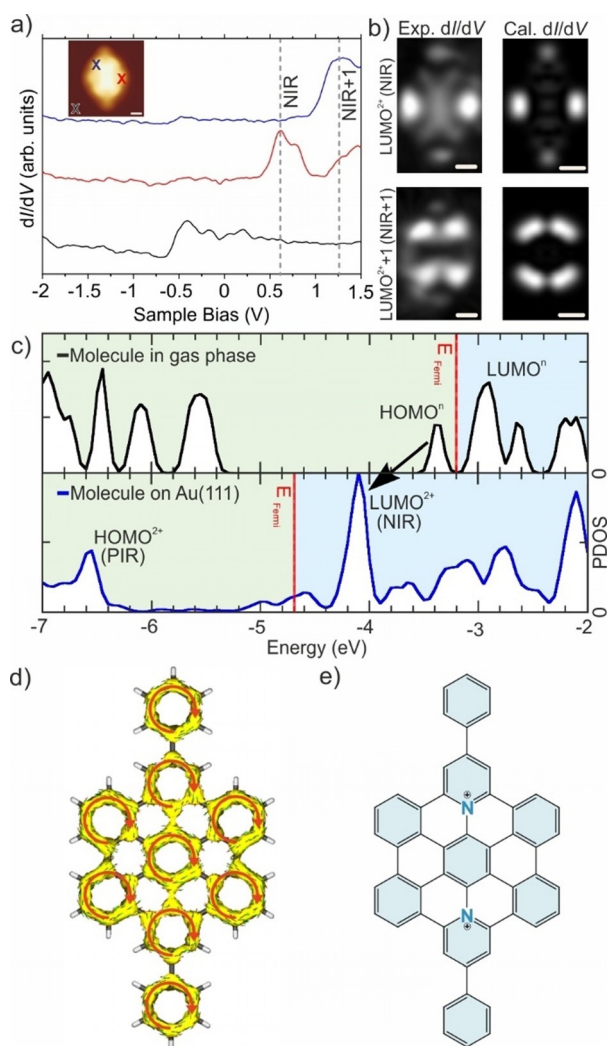


**Figure 3.** Electronic properties and aromaticity of **2** on Au(111). a)  $dI/dV$  spectra acquired on **2** at the position indicated by the red and blue crosses on the STM image shown in the inset. The black line corresponds to the reference spectra taken on the bare Au(111) surface. b) Constant-current  $dI/dV$  maps (left) of **2** on Au(111) and corresponding DFT-calculated LDOS maps of dicationic **2** in the gas phase (right) at the energetic positions corresponding to the LUMO (top left) and LUMO + 1 (bottom left) peaks, respectively. Open feedback parameters for the experimental  $dI/dV$  maps, LUMO:  $V_b = 0.6$  V,  $I_t = 250$  pA,  $V_{rms} = 20$  mV, LUMO + 1:  $V_b = 1.30$  V,  $I_t = 250$  pA,  $V_{rms} = 20$  mV. All scale bars: 0.5 nm. c) PDOS of **2** calculated in the gas phase for a neutral species (black curve) and the PDOS of **2** on the Au(111) surface (blue curve), where the HOMO clearly crossing the Fermi level can be discerned. d) ACID analysis of **2** calculated in the gas phase. Red arrows show the diatropic currents. Isovalue = 0.055 a.u. e) Kekulé structure of **2**. Blue filled benzenoid rings denote Clar sextets.

remained elusive. This could be attributed to the low energy position of the highest occupied molecular orbital above the Fermi level once the molecule is deposited on the Au(111) surface, provided a rigid shift of the energy level alignment of the frontier orbitals. Altogether, our analysis highlight the strong tendency to establish a +2 oxidation state of **2** on Au(111). In order to get an insight into the aromaticity of **2**, we have investigated the induced currents that result from an

applied magnetic field by evaluating the anisotropy of the induced current density (ACID). The plot depicted in Figure 3d clearly shows a clockwise current flowing along the diazahexabenzocoronene backbone as well as the two outer phenyl rings, where the most aromatic sextets exhibit local diatropic currents. Therefore, ACID calculations suggest that the +2 state imposes the presence of seven stabilizing clar sextets in the diazahexabenzocoronene backbone as depicted in the chemical sketch shown in Figure 3e (see Figure S4 for comparison with the ACID analysis of the neutral).

Recently, the synthesis of a similar nitrogen-doped NG to ours on the Ag(111) surface has been reported.<sup>[16]</sup> In that case, the obtained diazahexabenzocoronene contains a pyrazine unit, which serves as a localized  $8\pi$  antiaromatic (neutral) ring with a marginal charge transfer between the molecule and the metal silver surface, thus yielding a neutral NG. To assess the role of the nitrogen position (within its hexagonal lattice) in the capability of the molecular species to be charged on a metallic surface, we performed DFT simulations of the neutral species of the diazahexabenzocoronene containing a pyrazine unit in the gas phase and compare to results for the neutral form of **2**. Our computational results show a drastic difference in the energy level alignment with respect to vacuum between both species, which typically determines the overall charge transfer tendency. As a result, it should be expected a much stronger tendency to stabilize a charged form of **2** in comparison with the previously reported nanographene<sup>[16]</sup> (see Figure S5 for comparison). Therefore, in addition to size and edge structure, the introduction of nitrogen doping into the  $sp^2$ -carbon lattice of NGs opens possibilities for tailoring their intrinsic physical and chemical properties. Hereby, the location of such nitrogen atoms at specific positions of the NG lattice can promote the development of stable cationic nanostructures on surfaces.

Finally, to get further insights about the charge state of species **2** deposited on the Au(111) surface, we have carried out KPFM measurements.<sup>[43]</sup> Figure 4a displays acquired Kelvin parabolas, that is, the constant-height frequency shift dependence on the applied voltage bias on **2** adsorbed on the gold surface. Specifically, we observe a substantial variation of the local contact potential difference (LCPD), which shifts toward lower values with respect to the reference LCPD recorded on the bare Au(111) surface (Figure 4b). This LCPD shift concurs very well with the positive net charge of **2**.<sup>[44–48]</sup> Moreover, simulated KPFM images of fully relaxed **2** on the Au(111) match very well the experimental KPFM images acquired in a close tip-sample distance revealing submolecular resolution (see Figure S6 and methods section for further details).<sup>[48,49]</sup>

## Conclusion

In summary, we have demonstrated the on-surface synthesis of an unprecedented diazahexabenzocoronene derivative (**2**) via cyclodehydrogenation of precursor **1** on the Au(111) surface in an UHV environment. Its chemical and electronic structure have been elucidated by STM and nc-AFM acquired with CO-functionalized tips and STS meas-

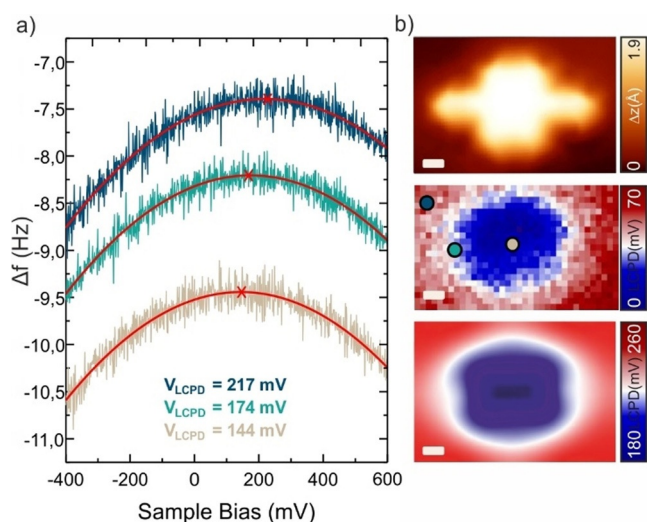


**Figure 4.** Charge distribution of **2**. a) Frequency shift dependence with  $V_{\text{bias}}$  voltage acquired with a CO-functionalized tip at the center (brown) and phenyl position (green) of **2**, as well as on the pristine Au(111) surface (blue) as shown in the STM image inset. The three measurements were acquired at the same tip-sample distance. b) STM image and KPFM map (top and middle panels, respectively) and corresponding simulation of **2** on Au(111) (bottom panel, calculated height = 11.5 Å), revealing the strong variation of the LCPD due to the presence of positively charged species **2**. Scale bars: 0.3 nm.

urements, respectively. The charge state of **2** has been investigated by STS and KPFM complemented with theoretical calculations, altogether revealing its positive dicationic charge. In addition, ACID calculations shows the aromatic character of **2**. The results reported herein illustrate the importance of the nitrogen doping and chemical design of NGs for tailoring their intrinsic physical and chemical properties, and the capability to stabilize net charges on metallic surfaces. We anticipate that our study will inspire future investigations of novel nanographene materials with heteroatom doping into their  $sp^2$ -carbon lattice with prospects in carbon-based optoelectronics.

## Acknowledgements

This project has received funding from Comunidad de Madrid [projects QUIMTRONIC-CM (Y2018/NMT-4783), MAD2D, and NanoMagCost], and Ministerio de Ciencia, Innovación y Universidades (projects SpOrQuMat, CTQ2017-83531-R, PID2019-108532GB-I00, and CTQ2016-81911-REDT). IM-DEA Nanociencia is appreciative of support from the “Severo Ochoa” Programme for Centers of Excellence in R&D (MINECO, grant SEV-2016-0686). The DFG-NSFC Joint Sino-German Research Project (EnhanceNano), Center for Advancing Electronics Dresden (cfaed), the European Social Fund, and the Federal State of Saxony (ESF-Project GRAPHD, TU Dresden) are acknowledged for financial support. The authors are grateful for the assistance of F. Drescher and Prof. E. Brunner (TU Dresden) for the HR-MS measurement. We acknowledge support from the Praemium Academie of the Academy of Science of the Czech Republic

and the CzechNanoLab Research Infrastructure supported by MEYS CR (LM2018110). P.J. acknowledges the support of the GACR 20-13692X. J.I.U. thanks the funding from the European Union’s Horizon 2020 research and innovation programme under the Marie Skłodowska-Curie grant agreement No. [886314]. A.M. and B.M. acknowledge the support from the Internal Student Grant Agency of the Palacký University in Olomouc, Czech Republic, IGA PrF 2021 031 and IGA PrF 2021 032, respectively. D. E. acknowledges funding from the European Research Council (ERC, grant 766555). Open Access funding enabled and organized by Projekt DEAL.

## Conflict of Interest

The authors declare no conflict of interest.

**Keywords:** cationic species · nanographenes · nc-AFM · scanning tunnelling microscopy · surface chemistry

- [1] K. S. Novoselov, *Science* **2004**, *306*, 666–669.
- [2] T. O. Wehling, K. S. Novoselov, S. V. Morozov, E. E. Vdovin, M. I. Katsnelson, A. K. Geim, A. I. Lichtenstein, *Nano Lett.* **2008**, *8*, 173–177.
- [3] K. S. Novoselov, V. I. Fal’ko, L. Colombo, P. R. Gellert, M. G. Schwab, K. Kim, *Nature* **2012**, *490*, 192–200.
- [4] X. Du, I. Skachko, A. Barker, E. Y. Andrei, *Nat. Nanotechnol.* **2008**, *3*, 491–495.
- [5] K. S. Novoselov, Z. Jiang, Y. Zhang, S. V. Morozov, H. L. Stormer, U. Zeitler, J. C. Maan, G. S. Boebinger, P. Kim, A. K. Geim, *Science* **2007**, *315*, 1379–1379.
- [6] C. Lee, X. Wei, J. W. Kysar, J. Hone, *Science* **2008**, *321*, 385–388.
- [7] A. Narita, X.-Y. Wang, X. Feng, K. Müllen, *Chem. Soc. Rev.* **2015**, *44*, 6616–6643.
- [8] X.-Y. Wang, A. Narita, K. Müllen, *Nat. Rev. Chem.* **2017**, *2*, 1–10.
- [9] R. Yang, C. Zhu, J. Meng, Z. Huo, M. Cheng, D. Liu, W. Yang, D. Shi, M. Liu, G. Zhang, *Sci. Rep.* **2013**, *3*, 2126.
- [10] J. Wu, W. Pisula, K. Müllen, *Chem. Rev.* **2007**, *107*, 718–747.
- [11] A. Narita in *Synthetic Methods for Conjugated Polymer and Carbon Materials* (Eds.: M. Leclerc, J.-F. Morin), Wiley-VCH, Weinheim, **2017**, pp. 183–228.
- [12] L. Gross, *Nat. Chem.* **2011**, *3*, 273–278.
- [13] Q. Shen, H.-Y. Gao, H. Fuchs, *Nano Today* **2017**, *13*, 77–96.
- [14] K. Müllen, J. P. Rabe, *Acc. Chem. Res.* **2008**, *41*, 511–520.
- [15] S. Mishra, M. Krzeszewski, C. A. Pignedoli, P. Ruffieux, R. Fasel, D. T. Gryko, *Nat. Commun.* **2018**, *9*, 1714.
- [16] X.-Y. Wang, M. Richter, Y. He, J. Björk, A. Riss, R. Rajesh, M. Garnica, F. Hennersdorf, J. J. Weigand, A. Narita, R. Berger, X. Feng, W. Auwärter, J. V. Barth, C.-A. Palma, K. Müllen, *Nat. Commun.* **2017**, *8*, 1948.
- [17] I. Piskun, R. Blackwell, J. Jornet-Somoza, F. Zhao, A. Rubio, S. G. Louie, F. R. Fischer, *J. Am. Chem. Soc.* **2020**, *142*, 3696–3700.
- [18] K. Nakamura, Q.-Q. Li, O. Krejčí, A. S. Foster, K. Sun, S. Kawai, S. Ito, *J. Am. Chem. Soc.* **2020**, *142*, 11363–11369.
- [19] D. Skidin, F. Eisenhut, M. Richter, S. Nikipar, J. Krüger, D. A. Ryndyk, R. Berger, G. Cuniberti, X. Feng, F. Moresco, *Chem. Commun.* **2019**, *55*, 4731–4734.
- [20] S. Mishra, T. G. Lohr, C. A. Pignedoli, J. Liu, R. Berger, J. I. Urgel, K. Müllen, X. Feng, P. Ruffieux, R. Fasel, *ACS Nano* **2018**, *12*, 11917–11927.

- [21] C. Rogers, C. Chen, Z. Pedramrazi, A. A. Omrani, H.-Z. Tsai, H. S. Jung, S. Lin, M. F. Crommie, F. R. Fischer, *Angew. Chem. Int. Ed.* **2015**, *54*, 15143–15146; *Angew. Chem.* **2015**, *127*, 15358–15361.
- [22] A. Sánchez-Grande, J. I. Urgel, L. Veis, S. Edalatmanesh, J. Santos, K. Lauwaet, P. Mutombo, J. M. Gallego, J. Brabec, P. Beran, D. Nachtigallová, R. Miranda, N. Martín, P. Jelínek, D. ěcija, *J. Phys. Chem. Lett.* **2020**, *11*, 330–336.
- [23] X.-Y. Wang, T. Dienel, M. Di Giovannantonio, G. B. Barin, N. Kharche, O. Deniz, J. I. Urgel, R. Widmer, S. Stolz, L. H. De Lima, M. Muntwiler, M. Tommasini, V. Meunier, P. Ruffieux, X. Feng, R. Fasel, K. Müllen, A. Narita, *J. Am. Chem. Soc.* **2017**, *139*, 4671–4674.
- [24] M. Di Giovannantonio, X. Yao, K. Eimre, J. I. Urgel, P. Ruffieux, C. A. Pignedoli, K. Müllen, R. Fasel, A. Narita, *J. Am. Chem. Soc.* **2020**, *142*, 12046–12050.
- [25] Q. Fan, D. Martin-Jimenez, S. Werner, D. Ebeling, T. Koehler, T. Vollgraff, J. Sundermeyer, W. Hieringer, A. Schirmeisen, J. M. Gottfried, *J. Am. Chem. Soc.* **2020**, *142*, 894–899.
- [26] K. Xu, J. I. Urgel, K. Eimre, M. Di Giovannantonio, A. Keerthi, H. Komber, S. Wang, A. Narita, R. Berger, P. Ruffieux, C. A. Pignedoli, J. Liu, K. Müllen, R. Fasel, X. Feng, *J. Am. Chem. Soc.* **2019**, *141*, 7726–7730.
- [27] S. Mishra, K. Xu, K. Eimre, H. Komber, J. Ma, C. A. Pignedoli, R. Fasel, X. Feng, P. Ruffieux, *Nanoscale* **2021**, *13*, 1624–1628.
- [28] I. C.-Y. Hou, Q. Sun, K. Eimre, M. Di Giovannantonio, J. I. Urgel, P. Ruffieux, A. Narita, R. Fasel, K. Müllen, *J. Am. Chem. Soc.* **2020**, *142*, 10291–10296.
- [29] J. Liu, S. Mishra, C. A. Pignedoli, D. Passerone, J. I. Urgel, A. Fabrizio, T. G. Lohr, J. Ma, H. Komber, M. Baumgarten, C. Corminboeuf, R. Berger, P. Ruffieux, K. Müllen, R. Fasel, X. Feng, *J. Am. Chem. Soc.* **2019**, *141*, 12011–12020.
- [30] J. Hieulle, E. Carbonell-Sanromà, M. Vilas-Varela, A. Garcia-Lekue, E. Guitián, D. Peña, J. I. Pascual, *Nano Lett.* **2018**, *18*, 418–423.
- [31] T. G. Lohr, J. I. Urgel, K. Eimre, J. Liu, M. Di Giovannantonio, S. Mishra, R. Berger, P. Ruffieux, C. A. Pignedoli, R. Fasel, X. Feng, *J. Am. Chem. Soc.* **2020**, *142*, 13565–13572.
- [32] S. Mishra, D. Beyer, R. Berger, J. Liu, O. Gröning, J. I. Urgel, K. Müllen, P. Ruffieux, X. Feng, R. Fasel, *J. Am. Chem. Soc.* **2020**, *142*, 1147–1152.
- [33] S. Mishra, X. Yao, Q. Chen, K. Eimre, O. Gröning, R. Ortiz, M. Di Giovannantonio, J. C. Sancho-García, J. Fernández-Rossier, C. A. Pignedoli, K. Müllen, P. Ruffieux, A. Narita, R. Fasel, *Nat. Chem.* **2021**, *13*, 581–586.
- [34] H. Wang, T. Maiyalagan, X. Wang, *ACS Catal.* **2012**, *2*, 781–794.
- [35] D. Guo, R. Shibuya, C. Akiba, S. Saji, T. Kondo, J. Nakamura, *Science* **2016**, *351*, 361–365.
- [36] Y. Xue, J. Liu, H. Chen, R. Wang, D. Li, J. Qu, L. Dai, *Angew. Chem. Int. Ed.* **2012**, *51*, 12124–12127; *Angew. Chem.* **2012**, *124*, 12290–12293.
- [37] Y. Wang, Y. Shao, D. W. Matson, J. Li, Y. Lin, *ACS Nano* **2010**, *4*, 1790–1798.
- [38] K. Xu, Y. Fu, Y. Zhou, F. Hennersdorf, P. Machata, I. Vincon, J. J. Weigand, A. A. Popov, R. Berger, X. Feng, *Angew. Chem. Int. Ed.* **2017**, *56*, 15876–15881; *Angew. Chem.* **2017**, *129*, 16092–16097.
- [39] W. Jun Lee, U. Narayan Maiti, J. Min Lee, J. Lim, T. Hee Han, S. Ouk Kim, *Chem. Commun.* **2014**, *50*, 6818–6830.
- [40] H. Kim, K. Lee, S. Ihl Woo, Y. Jung, *Phys. Chem. Chem. Phys.* **2011**, *13*, 17505–17510.
- [41] S. Kawai, S. Nakatsuka, T. Hatakeyama, R. Pawlak, T. Meier, J. Tracey, E. Meyer, A. S. Foster, *Sci. Adv.* **2018**, *4*, eaar7181.
- [42] L. M. Mateo, Q. Sun, K. Eimre, C. A. Pignedoli, T. Torres, R. Fasel, G. Bottari, *Chem. Sci.* **2021**, *12*, 247–252.
- [43] M. Nonnenmacher, M. P. O’Boyle, H. K. Wickramasinghe, *Appl. Phys. Lett.* **1991**, *58*, 2921–2923.
- [44] B. Schuler, S.-X. Liu, Y. Geng, S. Decurtins, G. Meyer, L. Gross, *Nano Lett.* **2014**, *14*, 3342–3346.
- [45] B. de la Torre, M. Švec, P. Hapala, J. Redondo, O. Krejčí, R. Lo, D. Manna, A. Sarmah, D. Nachtigallová, J. Tuček, P. Błoński, M. Otyepka, R. Zbořil, P. Hobza, P. Jelínek, *Nat. Commun.* **2018**, *9*, 2831.
- [46] B. Mallada, S. Edalatmanesh, P. Lazar, J. Redondo, A. Gallardo, R. Zbořil, P. Jelínek, M. Švec, B. de la Torre, *ACS Sustainable Chem. Eng.* **2020**, *8*, 3437–3444.
- [47] F. Albrecht, J. Repp, M. Fleischmann, M. Scheer, M. Ondráček, P. Jelínek, *Phys. Rev. Lett.* **2015**, *115*, 076101.
- [48] S. Kawai, A. Sadeghi, X. Feng, P. Lifan, R. Pawlak, T. Glatzel, A. Willand, A. Orita, J. Otera, S. Goedecker, E. Meyer, *ACS Nano* **2013**, *7*, 9098–9105.
- [49] F. Mohn, L. Gross, N. Moll, G. Meyer, *Nat. Nanotechnol.* **2012**, *7*, 227–231.

Manuscript received: September 1, 2021

Accepted manuscript online: September 21, 2021

Version of record online: October 21, 2021